Modelling of a semibatch polypropylene slurry reactor

M. Sau and Santosh K. Gupta*

Department of Chemical Engineering, Indian Institute of Technology, Kanpur 208016, India

(Received 25 March 1992; revised 27 January 1993)

Our previous polymeric multigrain model (PMGM) for the slurry polymerization of propylene is extended to account for the presence of gas–liquid mass transfer resistance and the gradual build-up of the monomer concentration in the liquid medium in an isothermal, semibatch reactor. Results are obtained for the situation where one starts with a pure n-heptane liquid medium. The Soave–Redlich–Kwong (SRK) equation is used for predicting gas–liquid equilibrium, and appropriate correlations are used to estimate mass transfer coefficients and interfacial areas for both the gas–liquid and liquid–solid interfaces. It is found that the initial transient in the monomer concentration leads to important effects on the rate of polymerization, the mean degree of polymerization ($\overline{DP}$) and the mean polydispersity index ($\overline{Q}$) and one must account for these phenomena. The effects of changing the various parameters are also studied. It is found that products with polydispersities higher than about 2.0 can be formed because of the presence of multiple activity catalyst sites and not because of diffusional limitations, at least for the parameters studied.

(Keywords: modelling; polypropylene; polymerization)

INTRODUCTION

Even though polypropylene is one of the most important commodity polymers, a sound understanding of the behaviour of reactors producing this polymer using Ziegler–Natta (ZN) catalysts[1] is lacking. This study is meant to narrow the gap in our understanding of polypropylene semibatch reactors. We attempt to model the operation of a semibatch slurry reactor during start-up, when the concentration of propylene builds up in the solvent (usually n-heptane). It is well documented[2,3] that the ZN catalyst particles break up during this early stage and that the timing and degree of fragmentation as well as the conditions at this time critically influence the subsequent polymerization. In this study we look at the early stages of polymerization in considerable detail. We account for the presence of mass transfer resistances at both the gas–liquid and liquid–solid interfaces. Floyd *et al.*[4] have found that these interfacial resistances could play an important role during polymerization when modern, high-activity catalysts are used. Our model, which accounts for various physicochemical phenomena which are operative, also provides a good starting point for the design of control systems, and sets the stage for the development of algorithms for optimization.

The semibatch reactor used in this study is shown schematically in *Figure 1*. The slurry taken initially in the reactor comprises a volume V_l of liquid solvent (usually n-heptane) and N_0 solid catalyst particles (all assumed to be spherical and having the same radius R_0). The vapour space (of volume V^*) above this slurry is occupied by some inert gas or (in this study) by propylene gas at 1 atm pressure. At time $t=0$, pure gaseous monomer (propylene) is bubbled into the reactor at a rate of $q_{m,in}$ mol s^{-1} (this rate could vary with time). The reactor is assumed to be well stirred (usually, a standard mixing tank geometry is taken, with a flat-blade disc turbine agitator used). Propylene dissolves partially in the solvent, and diffuses towards the catalyst particles through the solvent medium. The rate at which propylene transfers from the well-distributed gas bubbles to the liquid solvent will be controlled by the overall gas–liquid mass transfer coefficient and the gas–liquid interfacial area. If an excess of monomer is bubbled in, some of it ($q_{m,out}$ mol s^{-1}) will go to the vapour space at the top of the reactor. We thus have two regions which are in the vapour phase – one in the form of gas bubbles (forming a three-phase slurry), and the other at the top of the reactor, which we will refer to as the 'continuous gas phase'.

Monomer is transferred from the continuous liquid phase to the solid particles. Again, the liquid–solid mass transfer resistance and the total liquid–solid interfacial area will influence the rate of transfer. The monomer diffuses radially inwards inside the solid. During this process, polymerization takes place at the active sites of the catalyst. The polypropylene formed accumulates inside the solid particles, which grow with time. Very soon after the start of polymerization, the original catalyst breaks into several smaller fragments, called catalyst fragments, these being embedded in a continuum of polypropylene. These growing solid particles comprising polymer, catalyst fragments and diffusing monomer are called macroparticles. Several groups of workers[5–19] have studied the polymerization inside single macroparticles using a variety of models and techniques. Detailed discussions of these single-particle studies have been

* To whom correspondence should be addressed

0032-3861/93/214417-10

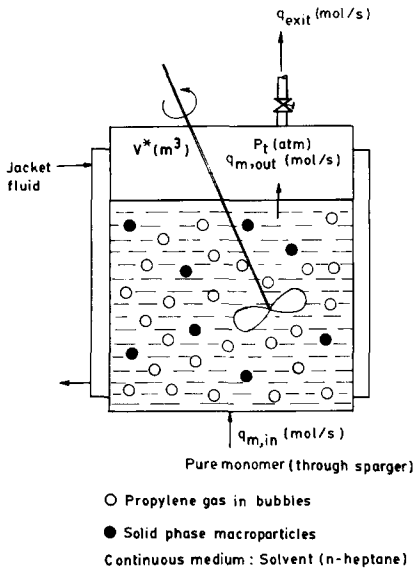

Figure 1 Schematic of a semibatch slurry polypropylene reactor

presented earlier[5–7,18,20] and are not repeated here for the sake of brevity.

At the beginning, most of the propylene bubbled in goes into building up the monomer concentration in the solvent. Slowly, the excess monomer starts accumulating (at a rate of $q_{m,out}$ mol s^{-1}) at the top of the reactor, and the pressure P_t builds up. One then needs to introduce monomer through the sparger at higher and higher pressures. As the concentration of monomer in the solvent builds up, one could reduce $q_{m,in}$. This, however, is not done (to avoid reduction in the mass transfer effects at the gas–liquid interface), and the pressure of the gas at the top of the reactor is usually maintained at some value by releasing vapour through a control valve, the monomer released being recycled. In this study q_{exit}, the rate of release of monomer from the reactor, is assumed to be such that the pressure P_t first builds up to a value P_{max} and is then maintained at this value.

In our study, we have assumed that heat transfer resistances are negligible in the semibatch reactor, and so the temperature is constant throughout (65°C). We have used our polymeric multigrain model (PMGM)[18,19] to account for the polymerization of propylene inside the macroparticles. The PMGM incorporates the salient features of the two families of models existing in the literature, and accounts for all the important physicochemical effects operative during polymerization.

FORMULATION

Solid phase

The equations describing the solid phase (growing macroparticles) are the same as used in our earlier studies[18–20] on single macroparticles, and are given in Table 1 of ref. 18. It is assumed in this study that all the N_0 macroparticles taken into the semibatch reactor are identical at any time t, and so the solution of these equations for a single macroparticle is sufficient. The diffusion of the monomer through the macroparticle is described by[18]

$$\frac{\partial M}{\partial t}=D_{ef}\frac{1}{r^2}\frac{\partial}{\partial r}\left(r^2\frac{\partial M}{\partial r}\right)-\mathscr{R} \tag{1a}$$

$$\text{at } r=0 \qquad \frac{\partial M}{\partial r}=0 \tag{1b}$$

$$\text{at } r=R_{N+2} \qquad D_{ef}\left(\frac{\partial M}{\partial r}\right)=k_{ls}(M_l-M) \tag{1c}$$

The various terms in these equations are defined in the Nomenclature. Equations (1) have to be solved along with the equations in Table 1 of ref. 18. In this work we have assumed that the chain transfer agent (H_2) is uniformly distributed in the macroparticle (i.e. the diffusivity of H_2 is very high).

Liquid phase

We now discuss the equation characterizing the well-mixed liquid phase (see *Figure 2*). The concentration M_l of monomer in the liquid phase is given by

$$V_l\frac{dM_l}{dt}=k_{gl}a_{gl}(V_g+V_l)(M^*_{l,i}-M_l)-k_{ls}a_{ls}(V_l+V_s)(M_l-M_{N+2}) \tag{2}$$

Equation (2) is applicable to the initial operation of the semibatch reactor, when the concentration of propylene builds up in the liquid solvent (n-heptane).

Gas bubble phase

The mass balance equation characterizing the 'gas bubble phase' (as contrasted to the gas above the slurry in the reactor) is given by

$$q_{m,out}=q_{m,in}-k_{gl}a_{gl}(V_g+V_l)(M^*_{l,i}-M_l) \tag{3}$$

Continuous gas phase

The pressure P_t in the continuous gas phase at the top of the reactor builds up with time due to the inflow of the gas bubbles. This is given by

$$\frac{dP_t}{dt}=\left(\frac{q_{m,out}-q_{exit}}{V^*}\right)\mathbb{R}T \tag{4}$$

where we have assumed ideal gas behaviour. Equations (3) and (4) lead to

$$\frac{dP_t}{dt}=\left[\frac{q_{m,in}-k_{gl}a_{gl}(V_g+V_l)(M^*_{l,i}-M_l)-q_{exit}}{V^*}\right]\mathbb{R}T \tag{5}$$

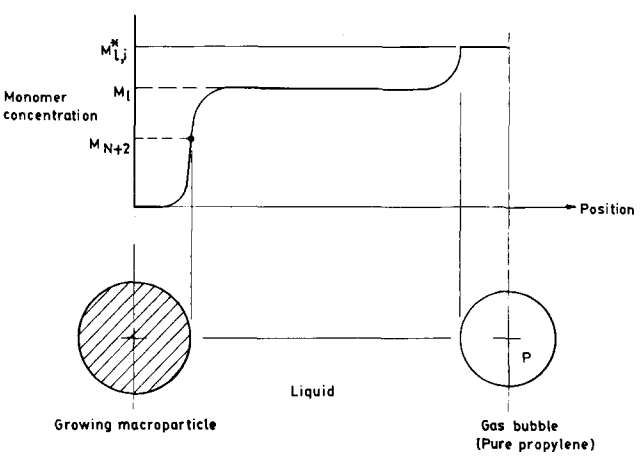

Figure 2 Variation of the monomer concentration with location at any time t

Table 1 Estimation[21 23] of a_{gl}, k_{gl} and V_g

Given $v_g(\approx 0.08\ m\ s^{-1})$ (a)

$$Q_g = \frac{\pi}{4} d_t^2 v_g \quad \text{(b)}$$

$$\frac{N_s d_i}{(\sigma g/\rho_l)^{1/4}} = 1.22 + 1.5\frac{d_t}{d_i} \quad \text{(c)}$$

$$Re_t = \frac{d_i^2 N_s \rho_l}{\mu_l} \quad \text{(d)}$$

$$W = 5\rho_l N_s^3 d_i^5 \quad \text{for } Re_t > 10^4 \quad \text{(e)}$$

$$\frac{W_g}{W} = 1 - 12.2\frac{Q_g}{N_s d_i^3} \quad \text{for } \frac{Q_g}{N_s d_i^3} < 0.037$$

$$= 0.62 - 1.85\frac{Q_g}{N_s d_i^3} \quad \text{for } 0.037 < \frac{Q_g}{N_s d_i^3} < 0.15$$

$$= 0.45 \quad \text{for } \frac{Q_g}{N_s d_i^3} > 0.15 \quad \text{(f)}$$

Assume v_{term}

$$a_0 = 1.44\left[\left(\frac{W_g}{V_l}\right)^{0.4}\left(\frac{\rho_l}{\sigma^3}\right)^{0.2}\right]\left(\frac{v_g}{v_{term}}\right)^{1/2} \quad \text{(g)}$$

For $Re_t^{0.7}\left(\frac{N_s d_i}{v_g}\right)^{0.3} \leq 30000$

$$a_{gl} = a_0 \quad \text{(h)}$$

For $Re_t^{0.7}\left(\frac{N_s d_i}{v_g}\right)^{0.3} > 30000$

$$a_{gl} = \left[(8.33\times 10^{-5}) Re_t^{0.7}\left(\frac{N_s d_i}{v_g}\right)^{0.3} - 1.5\right] a_0 \quad \text{(i)}$$

$$d_g^{0.35} = 1.90\left(\frac{V_l}{W}\right)^{0.4}\left(\frac{\sigma^3}{\rho_l}\right)^{0.2}\left(\frac{\mu_g}{\mu_l}\right)^{0.25}\left(\frac{a_{gl}}{6}\right)^{0.65} \quad \text{(j)}$$

$$\phi_g = \frac{a_{gl} d_g}{6} \quad \text{(k)}$$

Check v_{term} using[23]

$$K = \left[\frac{d_g g \rho_l (\rho_l - \rho_g)}{\mu_l^2}\right]^{1/3} \quad \text{(l)}$$

For $K < 2.6$ (Stokes region)[23]

$$v_{term} = \frac{g d_g^2 (\rho_l - \rho_g)}{18\mu_l} \quad \text{(m)}$$

For $2.6 < K < 68.9$ (ref. 23)

Assume $Re_g (1 < Re_g < 10^3)$

$$C_D = \left(\frac{24}{Re_g}\right)(1 + 0.14 Re_g^{0.7}) \quad \text{(n)}$$

$$v_{term} = \left(\frac{4g(\rho_l - \rho_g) d_g}{3 C_D \rho_l}\right)^{1/2} \quad \text{(o)}$$

Check $Re_g = \frac{d_g \rho_l v_{term}}{\mu_l}$ (p)

For $K > 68.9$ (ref. 23)

$$v_{term} = 1.75\left[\frac{d_g g(\rho_l - \rho_g)}{\rho_l}\right]^{1/2} \quad \text{(q)}$$

$$Ra = \frac{d_g^3 (\rho_l - \rho_g) g}{\mu_l D_l} \quad \text{(r)}$$

$$Sh_{gl} = 2.0 + 0.31 (Ra)^{1/3} \quad \text{(s)}$$

$$k_{gl} = \frac{Sh_{gl} D_l}{d_g} \quad \text{(t)}$$

$$V_g = V_l \frac{\phi_g}{1 - \phi_g} \quad \text{(u)}$$

$$q_{m,in} = \frac{1000}{22.4}\left(\frac{\pi}{4} d_t^2\right) v_g \frac{273}{T}\left[P_l(\text{atm}) + \frac{\rho_l g h}{1.013\times 10^5}\right] \quad \text{(v)}$$

Methodology of solution

The values of V_g, a_{gl} and k_{gl}, the total gas bubble volume, the gas–liquid interfacial area, and the gas–liquid mass transfer coefficient, respectively, can be estimated using a trial and error technique with the equations summarized[21–23] in *Table 1*. For a given liquid volume V_l, we first obtain a standard stirred-tank geometry (with $d_i = (1/3)d_t$, height of liquid $= d_t$). We then take a value for v_g, the superficial inlet gas velocity (v_g is related to the monomer sparging rate $q_{m,in}$). The volumetric feed rate of the gas Q_g is then calculated (using equation (b), *Table 1*). The rate of rotation N_s of the flat-blade disc turbine stirrer is estimated (equation (c), *Table 1*). Then the power required W for stirring pure liquid (no sparging) is estimated using equation (e) (for a high tank Reynolds number Re_t) of *Table 1*. The power required W_g in the presence of sparging is estimated using equation (f) of this table. A trial and error solution is then required to estimate the gas bubble diameter d_g or its terminal settling (rising) velocity v_{term}. A value of v_{term} is assumed and values of a_{gl} are estimated using equation (h) or (i) of *Table 1*. The quantity d_g and the gas volume fraction ϕ_g are estimated using equations (j) and (k) of *Table 1*. This d_g is checked against correlations for the terminal settling velocity given in equations (l) to (q) in *Table 1*. These equations are based on analytical expressions for the drag coefficients of spheres. Values of the converged d_g (and the corresponding ϕ_g) are used in equations (r) to (u) to give k_{gl} and V_g. The value of $q_{m,in}$ is obtained from equation (v) of *Table 1*.

The diffusivity D_l of propylene (prop) in liquid n-heptane (nC_7) is estimated using the Scheibel[22,24] correlation given in *Table 2*. Critical volumes $V_{c,i}$ for both these components are used in these equations. It is claimed[22] that this correlation gives better estimates than the Wilke–Chang[25] equation for diffusivities of organic solutes in organic solvents. Values of the various physical properties used in our study are given in *Table 3*.

The correlations used[4] for estimating a_{ls} and k_{ls} are given in *Table 4*. The quantity a_{ls} is easily estimated from the total number N_0 of macroparticles in the semibatch reactor using equation (a) of *Table 4*. The diameter d_s ($= 2R_{N+2}$) of the macroparticle is used to estimate its terminal settling velocity u_{term} using a trial and error procedure with equations (c) and (d) of *Table 4*. The converged value of the Reynold's number Re_s of the macroparticle (using u_{term}) is used in the Ranz–Marshall correlation (equation (f) of *Table 4*) to compute k_{ls}.

In order to integrate our system of equations, we first rewrite equations (1) in the finite difference form (for unequally spaced grid points[18]) to give a set of $(N+2)$ ordinary differential equations (ODEs) for M_i, the monomer concentrations at each of the $(N+2)$ different computational grid points shown in Figure 1 of ref. 18. These are given in Table 2 of ref. 18 (with M_b replaced by M_l). In addition to these $(N+2)$ ODEs, we have two

Table 2 Estimation of D_l (Scheibel correlation[22,24])

$V_i'' = 0.285 V_{c,i}^{0.148}$ i = prop, nC_7 (Tyn and Calus equation[22]) (a)

$$K'' = (8.2\times 10^{-8})\left[1 + \left(\frac{3V''_{nC7}}{V''_{prop}}\right)^{2/3}\right] \quad \text{(b)}$$

$$D_l \equiv D_{prop\ nC7} = \frac{K'' T}{\mu_l V''^{1/3}_{prop}} \quad \text{(c)}$$

Table 3 Values of physical and thermodynamic properties used

Property	Propylene	n-Heptane
Surface tension[22] σ	–	2.014×10^{-2} N m^{-1} (liquid)
Density[22] ρ_g, ρ_l	$f(P_t, T)$ from ideal gas law (gas)	683.7 kg m^{-3} (liquid)
Viscosity[23] μ_l, μ_g	9.25×10^{-6} kg m^{-1} s^{-1} (gas)	2.8×10^{-4} kg m^{-1} s^{-1} (liquid)
Critical volume[26,27] V_c	1.81×10^{-6} m^3 mol^{-1}	432.3×10^{-6} m^3 mol^{-1}

more coupled ODEs (equations (2) and (5) for M_1 and P_t). The equilibrium relationship between $M^*_{l,i}$ and P_t is an algebraic one, and is given by a set of four cubic spline expressions given in *Table 5*. These expressions have been obtained by a curve fit of the vapour–liquid equilibrium information on the propylene–n-heptane system at 65°C (the temperature used in this study) from the Soave–Redlich–Kwong (SRK) equation of state[26–28].

The numerical procedure involves the evaluation of the entire monomer concentration profile and P_t at time $t+\Delta t$ by integrating the $(N+4)$ coupled ODEs for M_i $(i=1, 2, \ldots, N+2)$, M_1 and P_t from time t to $t+\Delta t$. Gear's method (using subroutine D02EBF of the NAG library) is used for this purpose. The exact numerical procedure used (including decoupling of the equations into two sets solved separately) is similar to that used in our previous work[18–20,28]. For small times of polymerization[19] (below 0.002 h), we have used $\Delta t = \Delta t_1 = 10^{-4}$ h. After $t = 0.002$ h $(\equiv t_1)$, we use $\Delta t = \Delta t_2 = 10^{-3}$ h.

While performing the integration of the $(N+4)$ coupled ODEs, we have built in the following additional options.

1. For $P_t < P_{max}$.

   (i) Case 1: $k_{gl}a_{gl}(V_g + V_l)(M^*_{l,i} - M_l) < q_{m,in}$ (6)

   Under this condition, equations (2) and (5) are used as such and q_{exit} is put as zero.

   (ii) Case 2: $k_{gl}a_{gl}(V_g + V_l)(M^*_{l,i} - M_l) \geq q_{m,in}$ (7)

   Under this condition, equations (2) and (5) are replaced by the following equations

$$\frac{dM_1}{dt} = \frac{q_{m,in} - k_{ls}a_{ls}(V_l + V_s)(M_1 - M_{N+2})}{V_l} \quad (8a)$$

$$\frac{dP_t}{dt} = 0 \quad (8b)$$

$$q_{exit} = 0 \quad (8c)$$

   This prevents more monomer from being transferred to the liquid than that fed into the reactor. This second option is used only in the first few minutes of operation for the conditions used in this study.

2. For $P_t > P_{max}$.

   We use the equation for dM_l/dt as given above for cases 1 and 2. In addition, we use the following equations for case 1

$$\frac{dP_t}{dt} = 0 \qquad P_t = P_{max} \quad (9a)$$

$$q_{exit} = q_{m,in} - k_{gl}a_{gl}(V_g + V_l)(M^*_{l,i} - M_l) \quad (9b)$$

   Under the operating conditions studied in this work, $q_{m,in}$ was always found to be larger than $k_{gl}a_{gl}(V_g + V_l)(M^*_{l,i} - M_l)$ (i.e. case 1) after the first few minutes of operation. If, however, this condition is violated and we have case 2 with $P_t > P_{max}$, we could use

$$q_{exit} = 0$$

$$\frac{dP_t}{dt} = [-k_{gl}a_{gl}(V_g + V_l)(M^*_{l,i} - M_l) + q_{m,in}]RT/V^* \quad (10)$$

   to account for the transfer of propylene from the vapour space above the slurry to the liquid medium (the equations for estimating k_{gl} and a_{gl} account for the entrapment of gas from the space above). This option, though present in our program, was not actually used. We have also made the concentration M_i inside the macroparticles as zero whenever they are found to be negative. This option is used in the initial stages due to the high local rates of reaction.

Table 4 Correlations[4] used for estimating a_{ls} and k_{ls}

$$a_{ls} = \frac{4\pi R^2 N_0}{V_l + V_s} \quad (a)$$

Assume Re_s (b)

Calculate u_{term}

$$u_{term} = \frac{g d_s^2(\rho_p - \rho_l)}{18\mu_l} \qquad \text{for } Re_s < 0.4$$

$$u_{term} = \left[\frac{4g^2(\rho_p - \rho_l)^2}{225\rho_l\mu_l}\right]^{1/3} d_s \qquad \text{for } 0.4 < Re_s < 500$$

$$u_{term} = \left[\frac{3.1 g d_s(\rho_p - \rho_l)}{\rho_l}\right]^{1/2} \qquad \text{for } Re_s > 500 \quad (c)$$

Check $Re_s = \frac{d_s u_{term}\rho_l}{\mu_l}$ (d)

$$Sc = \frac{\mu_l}{\rho_l D_l} \quad (e)$$

$Sh_{ls} = 2 + 0.6 Sc^{1/3} Re_s^{1/2}$ (Ranz–Marshall equation) (f)

$$k_{ls} = \frac{Sh_{ls} D_l}{d_s} \quad (g)$$

RESULTS AND DISCUSSION

The Soave–Redlich–Kwong (SRK)[26,27] equation of state is used for the binary system, propylene–n-heptane, to compute the value of $M^*_{l,i}$, the equilibrium concentration of propylene in n-heptane at the gas–liquid interface. The values of $M^*_{l,i}$ are obtained[28] at different pressures P_t at 65 °C. These SRK values of $M^*_{l,i}$ are then curve fitted using simpler equations for routine use. Four different cubic splines in different ranges of pressure are obtained and are given in *Table 5*. *Table 6* shows values of $M^*_{l,i}$ obtained from these two techniques at different values of P_t. It is observed that the spline fit is acceptable. It may be added that even though we have used the SRK equation for a binary system to predict $M^*_{l,i}(P_t)$, we have neglected the vaporization of n-heptane into the gas bubbles and

Table 5 Relationships between P_t and $M^*_{l,i}$ using cubic splines[a]

$$M^*_{l,i} = 0.0064 + 0.28444(P_t - 0.35) + 0.00051(P_t - 0.35)^3 \quad 0.35 \leqslant P_t \leqslant 5 \quad \text{(a)}$$

$$M^*_{l,i} = 1.37995 + 0.3148(P_t - 5.0) + 0.00706(P_t - 5)^2 - 0.00083(P_t - 5)^3 \quad 5.0 \leqslant P_t \leqslant 10 \quad \text{(b)}$$

$$M^*_{l,i} = 3.02633 + 0.41416(P_t - 10) + 0.00544(P_t - 10)^2 + 0.0006(P_t - 10)^3 \quad 10 \leqslant P_t \leqslant 20 \quad \text{(c)}$$

$$M^*_{l,i} = 6.68274 + 0.32301(P_t - 20) + 0.00367(P_t - 20)^2 + 0.00024(P_t - 20)^3 \quad 20 \leqslant P_t \leqslant 25 \quad \text{(d)}$$

[a] P_t in atm and $M^*_{l,i}$ in mol l^{-1}; $T = 65°C$

Table 6 SRK and spline values of $M^*_{l,i}$ ($T = 65°C$) at different P_t

	SRK			Spline	
P_t (atm)	x_{C_3}[a]	y_{C_3}[a]	$10^{-3}M^*_{l,i}$ (mol m^{-3})	$10^{-3}M^*_{l,i}$ (mol m^{-3})	Pressure range for spline used (*Table 7*)
0.35	0.00113	0.0653	0.00640	0.00640	
0.50	0.0085	0.3453	0.04835	0.0491	
0.75	0.0207	0.5637	0.11861	0.1202	
1.00	0.03289	0.6731	0.18930	0.1914	$0.35 \leqslant P_t \leqslant 5$ atm
2.00	0.08091	0.8377	0.47641	0.4780	
3.00	0.1279	0.8927	0.77052	0.7697	
4.00	0.17397	0.9203	1.07169	1.0694	
5.0	0.219	0.937	1.37995	1.37995	
6.0	0.2631	0.9481	1.69531	1.70098	
7.0	0.3063	0.9561	2.01772	2.03113	$5 \leqslant P_t \leqslant 10$ atm
8.0	0.349	0.962	2.34713	2.36541	
9.0	0.3899	0.967	2.68340	2.69881	
10.0	0.430	0.971	3.02633	3.02633	
12.0	0.5087	0.9767	3.73098	3.83336	
14.0			4.45751	4.59969	$10 \leqslant P_t \leqslant 20$ atm
16.0			5.19969	5.32815	
18.0			5.94715	6.02156	
20.0			6.68274	6.68274	
21.0			7.03783	7.00232	
22.0			7.37811	7.31601	
23.0			7.69713	7.62530	$20 \leqslant P_t \leqslant 25$ atm
24.0			7.98669	7.93165	
25.0			8.23653	8.23653	

[a] x_{C_3} and y_{C_3} represent mole fractions of propylene in equilibrium liquid and vapour respectively

have neglected the gas–film mass transfer resistance. This is quite a good approximation since it is found that the mole fraction of n-heptane in the vapour phase is below about 0.1 at P_t as low as 3 atm, and decreases still further as P_t is increased (its value being only 0.022 for $P_t = 12.5$ atm). It may be added that neglecting the mass transfer of n-heptane to the gas bubbles has an opposite effect to neglecting the decrease in the gas bubble size, and the errors due to the use of these two approximations tend to cancel out. We have also used the ideal gas law to estimate the density of pure propylene in equation (5) instead of using the SRK equation of state. This is not expected to lead to any significant error.

The values of the reactor operating conditions and parameters used in this study are given in *Table 7*. Some of these reference values are the same as those used by Sarkar and Gupta[19]. The rate constants are chosen to correspond to catalysts of relatively high activity. The value of $k_{tr}[H_2]^{1/2}$ is chosen to give polymers having number-average molecular weights in the region[29] of 200 000. It may be emphasized that $k_{tr}[H_2]^{1/2}$ really sums up the effects of all the chain transfer steps (to monomer,

Table 7 Reference values of the parameters and operating conditions

Parameter	Value	Units
C^*	3.2	mol site $(m^3$ catalyst$)^{-1}$
D_s	10^{-10}	$m^2\ s^{-1}$
k_p	2.5	m^3 (mol site)$^{-1}\ s^{-1}$
$k_{tr}[H_2]^{1/2}$	1.86	s^{-1}
N	36	
N_0	10^{12}	
P_{max}	1.266×10^6 (12.5)	Pa (atm)
P_t ($t = 0$)	1.013×10^5	Pa (pure propylene)
R_0 (before breakage)	1.15×10^{-5}	m
$R_{c,i}$ (after breakage)	2.0×10^{-7}	m (uniform)
$\mathbb{R}$	8.314	J $mol^{-1}\ K^{-1}$
T	338.0	K
V^*	4.0	m^3
v_g	0.08	$m\ s^{-1}$
V_l	20.0	m^3
ρ_c	2260	kg m^{-3}
ρ_p	900	kg m^{-3}
Computational parameters		
Δt_1	10^{-4}	h
Δt_2	10^{-3}	h
t_1	0.002	h

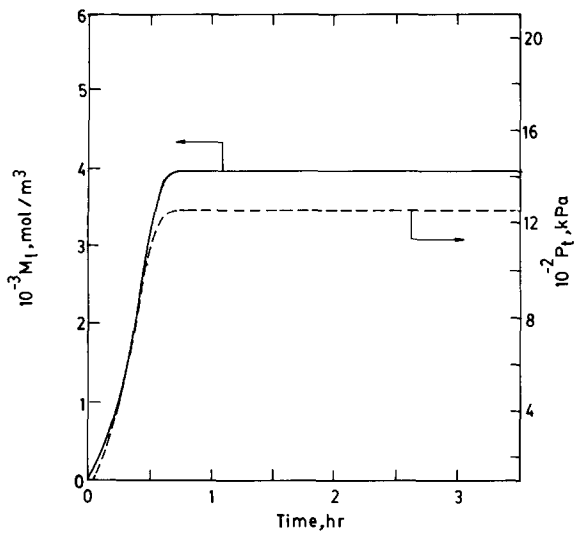

Figure 3 Variation of M_l and P_t with time (T=65°C). Note the initial transients in M_l. Reference conditions used as given in *Table 7*

hydrogen, cocatalyst, etc.) actually occurring in the reactor. The reactor volumes, catalyst loading, etc. in *Table 7* are values which are typically used in industry[29].

Several tests were made to check the correctness of our computer code. We obtained results for the special case when the gas–liquid interfacial diffusional resistance is assumed to be zero (i.e. $dM_l/dt=0$ and $dP_t/dt=0$), M_l to be constant at 4×10^3 mol m^{-3}, and $k_{ls}=10^{-3}$ m s^{-1}). These results matched those obtained from the computer code of Sarkar and Gupta[19]. We also changed the values of the computational parameters (e.g. TOL in D02EBF, Δt_1, Δt_2, t_1, etc.) and found imperceptible changes in our results. The time taken for a single run of 3.5 h polymerization time was 48 s on an HP 9000/850 S computer, without using clubbing of shells[19].

Our first simulation run corresponds to using 20 m^3 of pure n-heptane ($M_l=0$) in the reactor at the beginning ($t=0$). A total of 10^{12} catalyst particles (spherical) each having a radius (prior to fragmentation) R_0 of 1.15×10^{-5} m is taken into the reactor. Gaseous propylene is then bubbled in, and its superficial velocity v_g is maintained at a constant 0.08 m s^{-1}, as recommended by Treybal[21] for achieving good mass transfer rates. The value of P_{max} is taken to be 12.66×10^5 Pa. *Figure 3* shows how the monomer concentration M_l builds up in the liquid phase (referred to as 'transient'). It is observed that it takes a reasonable amount of time ($\sim$0.7 h) for M_l to build up to its final value of 3972.9 mol m^{-3} (corresponding to $P_t=P_{max}=12.66\times10^5$ Pa). Most theoretical studies reported up to now have neglected this relatively slow build-up of the monomer concentration, and have assumed M_l to be constant. Neglecting the transients in M_l is likely to lead to significant errors in prediction since it is well known[2,3] that catalyst fragmentation occurs during the initial period, and that conditions existing inside the solid macroparticles then determine the exact nature of fragmentation (which, in turn, determines the subsequent polymerization). The present study is thus an improvement over earlier studies in that it accounts for the variation of M_l with time in real reactors.

The build-up of pressure above the slurry is also shown in *Figure 3*. It is assumed that the gas space above the slurry is filled initially with pure propylene at 1.013×10^5 Pa. The pressure P_t increases with time and is maintained at P_{max} ($=12.66\times10^5$ Pa), once this value is attained, through the release of vapour at a rate q_{exit} (mol s^{-1}). The latter is plotted in *Figure 4*, along with $q_{m,in}$. It is possible to reduce q_{exit} and reduce monomer recycling costs, but this would lead to a lowering of $q_{m,in}$ and a corresponding undesirable reduction in the mass transfer coefficient k_{gl}. One could envisage, however, an optimal $q_{m,in}$ history, but in the present study we do not focus on this issue (but keep v_g constant at 0.08 m s^{-1}). It may be noted from *Figures 3* and *4* that P_t initially remains constant at 1.013×10^5 Pa for a short interval of time (approximately 0.05 h) before increasing. During this time, all of the monomer fed into the reactor is transferred to the slurry, and none of it goes into the vapour space above the slurry. The value of $q_{m,in}$ remains constant during this interval. After this period, only a part of the monomer sparged in is transferred to the slurry, while some of it goes to the vapour space at the top. This leads to an increase in P_t and $q_{m,in}$ (an increase in the sparging pressure leads to higher molar feed rates even though v_g is constant).

Figure 5 (solid curve) shows the effect of the transient in the monomer concentration on the (instantaneous) rate of polymerization as well as on the size of the polymer particle (which reflects the yield). The corresponding curves in the absence of this transient, using constant values for M_l (3972.9 mol m^{-3}) and k_{ls} (4.66×10^{-4} m s^{-1}, the value at $t=3.5$ h for the conditions corresponding to the solid curve), are also shown. The initial value of monomer concentration M_i inside the catalyst particles is zero for all cases. The difference between the curves reflects the compounded effects of incorporating the gas–liquid mass transfer resistance in the model, as well as that of the gradual build-up of the concentration M_l of monomer in the liquid associated with the increase in the pressure P_t. It is interesting to observe that even though it takes only about 0.7 h for M_l and P_t to build up to their constant values, their effects persist for later times as well. Neglecting the transients leads to an overprediction of the final yield by about 4%. A similar overprediction of the mean degree of polymerization by as much as 11% (by neglecting the transient in M_l) is

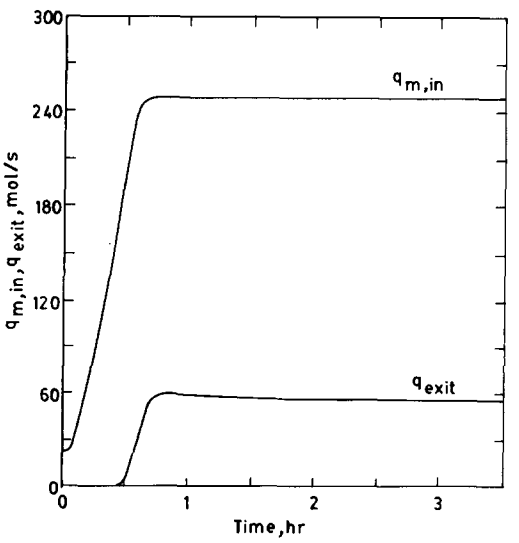

Figure 4 Variation of $q_{m,in}$ and q_{exit} with time (conditions as for *Figure 3*)

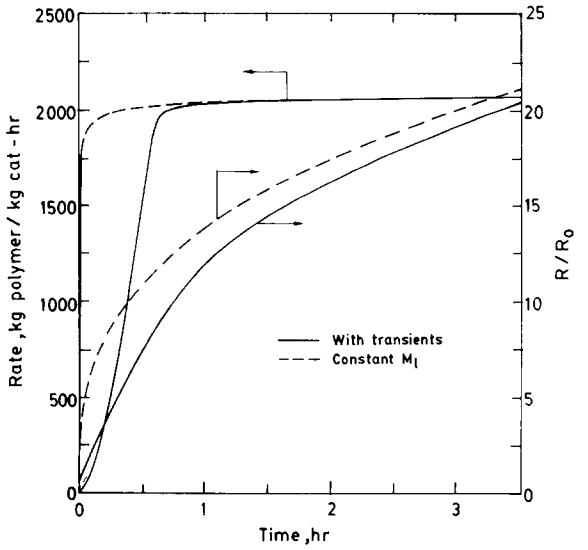

Figure 5 Instantaneous rate of polymerization and dimensionless size of particles as a function of time (conditions as for *Figure 3*)

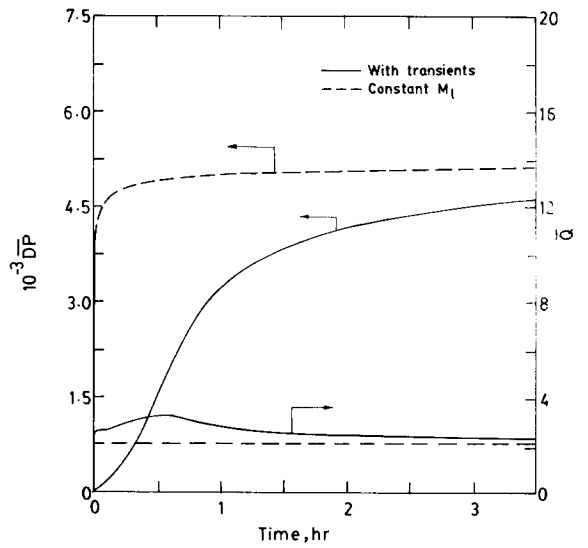

Figure 6 Variation of the average degree of polymerization and average polydispersity index with time (conditions as for *Figure 3*)

observed in *Figure 6*. The importance of accounting for the gas–liquid mass transfer resistance and the associated delayed build-up of the monomer concentration in the liquid is thus established.

The mass transfer coefficient k_{ls} decreases with time to about 4.7×10^{-4} m s^{-1} while a_{ls} increases first and, after a shallow maximum, then decreases slowly to about 0.85 m^2 m^{-3} at $t = 3.5$ h. In our earlier work[18,19], we had used constant values for both these parameters. The gas–liquid mass transfer coefficient k_{gl} is found to be relatively constant at 4.9×10^{-4} m s^{-1} because the superficial inlet gas velocity v_g is constant. For the same reason, a_{gl} is almost constant at about 2.96×10^{-2} m^2 m^{-3}.

The effects of varying some of the important operating conditions and parameters were also studied. *Figure 7* shows that increasing k_p from 2.5 m^3 mol^{-1} s^{-1} (reference value) to 3 m^3 mol^{-1} s^{-1} (while keeping all other parameters at their reference values) delays the build-up of monomer concentration in the n-heptane medium because of its higher consumption inside the solid particles. *Figure 8* shows the sensitivity of the rates and yields to k_p. Increasing k_p (keeping $k_{tr}[H_2]^{1/2}$ unchanged) leads to products having $\overline{DP}$ about 15% higher. Increases in the active site concentration C^* should lead to almost similar effects since the terms k_p and C^* mostly (but not always) occur together in the equations as k_pC^*.

An important drawback in most studies on the simulation of polymerization reactors, particularly those involving many phases, is the lack of good correlations for estimating mass (and heat) transfer correlations. We decided to check whether this is important for slurry propylene reactors as well. We made k_{gl} five times its value predicted from the equations in *Table 1*, and found that this leads to negligible increases in the rate and $\overline{DP}$. Hence, we infer that these results are not too sensitive to the correlations used for estimating the gas–liquid mass transfer parameters. Since k_{gl} and a_{gl} occur together in the equations, similar inferences can be made for the effect of changing a_{gl}. Changing k_{ls} (arbitrarily) to five times the value predicted from the Ranz–Marshall equation

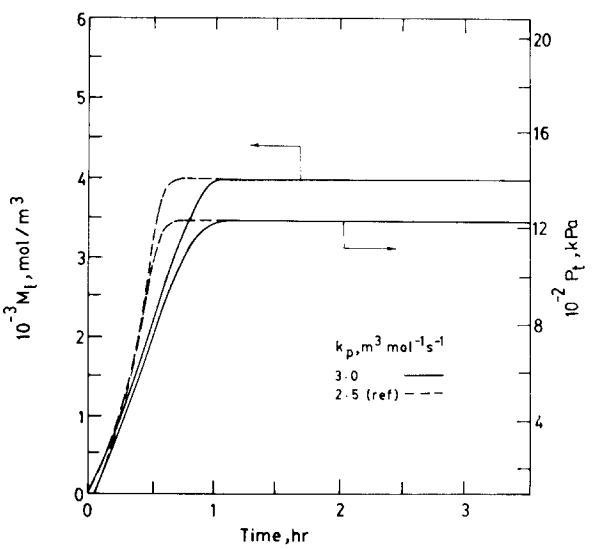

Figure 7 Effect of increasing k_p on M_i and P_t. All other parameters are at their reference values (*Table 7*)

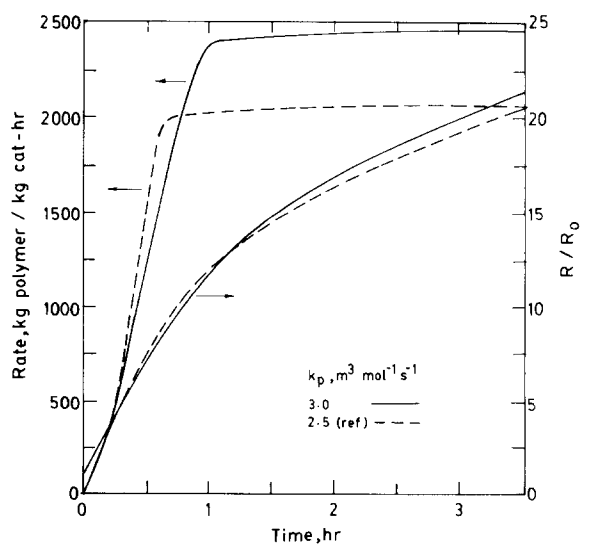

Figure 8 Effect of increasing k_p on the rate and yield

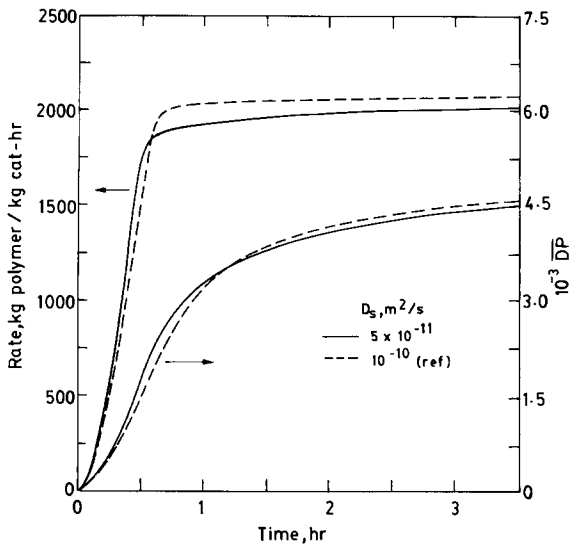

Figure 9 Effect of decreasing D_s from reference value of 10^{-10} m^2 s^{-1} to 5×10^{-11} m^2 s^{-1} on rate and $\overline{DP}$

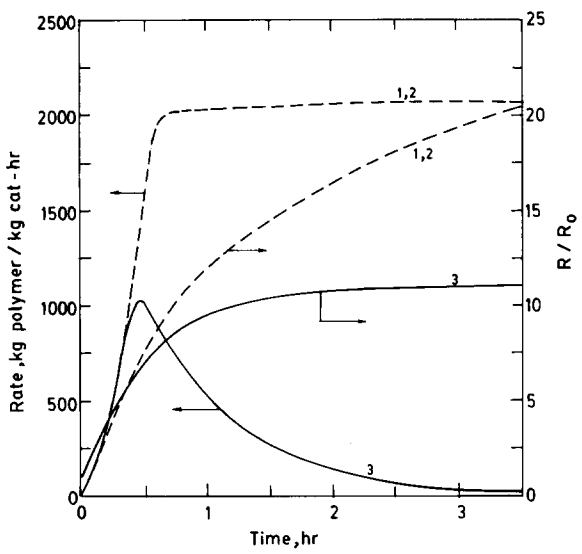

Figure 10 Effect of incorporating two kinds of catalyst sites with (curves 3) and without (curves 2) first-order decay on the rate and yield. $k_{p,1} = 1.0$ m^3(mol site)$^{-1}$ s^{-1}; $k_{p,2} = 7.0$ m^3(mol site)$^{-1}$ s^{-1}; $C_1^* = 2.4$ mol site (m^3 catalyst)$^{-1}$; $C_2^* = 2.8$ mol site (m^3 catalyst)$^{-1}$; $t_{1/2}$ (first order) = 0.5 h for both sites. Dashed curves are indistinguishable from reference results (for single site, curves 1)

(*Table 4*) also leads to insignificantly higher rates and $\overline{DP}$s. We thus conclude that we can use any reasonable correlation for estimating the mass transfer effects, at least for catalysts having relatively high activity.

The effect of reducing the monomer diffusivity D_s from the reference value of 10^{-10} m^2 s^{-1} to 5×10^{-11} m^2 s^{-1} is shown in *Figure 9*. The reaction rate over most of the polymerization is reduced. The product $\overline{DP}$ is also slightly reduced. There is imperceptible difference in the polydispersity index. It is thus confirmed that for catalysts of relatively high activity the value of $\bar{Q}$ is close to 2.0 for single-site catalysts. Values of $\bar{Q}$ far above 2.0 can therefore be attributed primarily to the presence of multiple activity catalysts (which have sites having different values of k_p, etc.). It may be mentioned here that in our model only a single diffusion parameter D_s is used. Its reference value of 10^{-10} m^2 s^{-1} is taken to lie between the two diffusivities (for macroparticles and microparticles) used in the multigrain model of Ray and coworkers[4,11,13–15,17].

It was also found in our study that changing the number N of shells from 36 to 30 while keeping R_0 constant (i.e. $R_{c,i}$ is increased simultaneously as N is decreased) does not change the results perceptibly, even for $D_s = 5 \times 10^{-11}$ m^2 s^{-1}. This does not necessarily imply that the effect of catalyst particle breakage (at values of t larger than zero) is negligible. We need to modify our single-particle model considerably to account for particle breakage in an appropriate manner to find out the answer to this interesting question. Since the polymer is formed first in the outer regions, particle breakage would take place there before the inner regions break up. One could modify our model to account for such a sequential break-up of the catalyst particle somewhat along the lines followed by Ferrero and Chiovetta[2,3]. We believe that interesting results would be obtained, but this was not the focus of the present study.

Figures 10 and *11* show some results for multiple activity catalysts. Two kinds of active sites are assumed to be present in the catalyst. The values[19] of $k_{p,1}$, $k_{p,2}$, C_1^* and C_2^* are selected as

$$k_{p,1} = 1.0 \text{ m}^3 \text{ (mol site)}^{-1} \text{ s}^{-1}$$
$$k_{p,2} = 7.0 \text{ m}^3 \text{ (mol site)}^{-1} \text{ s}^{-1}$$
$$C_1^* = 2.4 \text{ mol site (m}^3 \text{ catalyst)}^{-1}$$
$$C_2^* = 0.8 \text{ mol site (m}^3 \text{ catalyst)}^{-1} \qquad (11)$$

These values are such that $\sum_{i=1}^{2} k_{p,i} C_i^*$ is equal to $k_p C^*$ for the single-site catalyst in the reference run. All other parameters are at their reference values. It is found (curves 1, 2) that the rate and yield are almost unchanged from the single-site reference results. This is not surprising since $\sum_{i=1}^{2} k_{p,i} C_i^*$ has been chosen to be the same as $k_p C^*$ for the single-site catalyst. *Figure 11* shows that $\overline{DP}$ is also quite insensitive to multiple activity sites (curves 1 and 2) under these conditions, but that a higher (curve 2) polydispersity product is obtained with multisite catalysts than with single-site catalysts (curve 1). Introduction of first-order decay with a half-life of 0.5 h

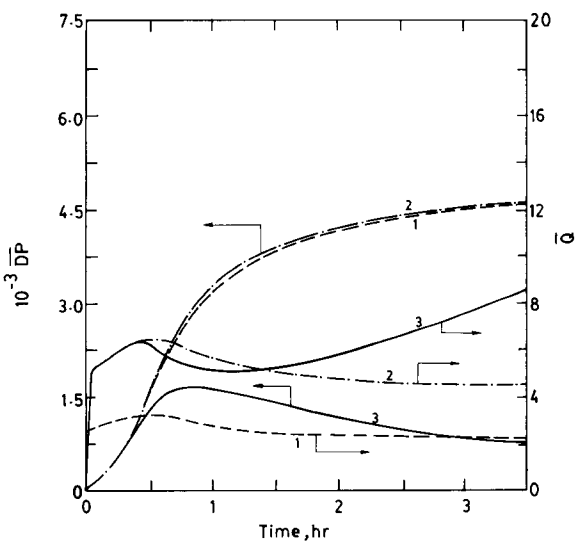

Figure 11 Effect of two-site catalysts without decay (curves 2) and with first-order decay (curves 3). Single-site reference results (curves 1) are also shown. Values of parameters are as for *Figure 10*

for both sites (curves 3 in *Figures 10* and *11*) leads to polydispersity indices of the final product as high as 8.5 for the parameter values studied. It may be added that clubbing of shells[19] was used to generate multisite catalyst results.

CONCLUSIONS

A detailed simulation of propylene polymerization (slurry) was carried out in a semibatch reactor. This model incorporated various physicochemical aspects of the ZN polymerization of propylene. This model differed from our previous work[18,19] in that it accounted for diffusional limitations on the gas–liquid side, as well as the slow build-up of the monomer concentration in the liquid phase. The results showed that incorporating these effects influenced the rate of polymerization, $\overline{DP}$ and $\bar{Q}$ significantly. It was also observed that even though the transient in M_l lasted for only about 0.7 h, the rate of polymerization, $\overline{DP}$ and $\bar{Q}$ were affected till much later times. It was found that values of the polydispersity index far above 2.0 could be explained in terms of the presence of multisite catalysts rather than diffusional effects. The influence of the important parameters was also studied.

REFERENCES

1 Natta, G., Pino, P., Mazzanti, G., Guannini, U., Mantica, E. and Peraldo, M. *J. Polym. Sci.* 1957, **26**, 120
2 Ferrero, M. A. and Chiovetta, M. G. *Polym. Eng. Sci.* 1991, **31**, 886
3 Ferrero, M. A. and Chiovetta, M. G. *Polym. Eng. Sci.* 1991, **31**, 904
4 Floyd, S., Choi, K. Y., Taylor, T. W. and Ray, W. H. *J. Appl. Polym. Sci.* 1986, **31**, 2231
5 Choi, K. Y. and Ray, W. H. *J. Macromol. Sci., Rev. Macromol. Chem. Phys.* 1985, **C25** (1), 57
6 Galvan, R. and Tirrell, M. *Chem. Eng. Sci.* 1986, **41**, 2385
7 Galvan, R. and Tirrell, M. *Comput. Chem. Eng.* 1986, **10**, 77
8 Schmeal, W. R. and Street, J. R. *AIChE J.* 1971, **17**, 1188
9 Buls, V. W. and Higgins, T. L. *J. Polym. Sci. (A-1)* 1970, **9**, 1037
10 Brockmeier, N. F. and Rogan, J. B. *AIChE Symp. Ser.* 1976, **72** (160), 28
11 Nagel, E. J., Kirillov, V. A. and Ray, W. H. *Ind. Eng. Chem., Prod. Res. Dev.* 1980, **19**, 372
12 Singh, D. and Merrill, R. P. *Macromolecules* 1971, **4**, 599
13 Choi, K. Y. and Ray, W. H. *J. Appl. Polym. Sci.* 1985, **30**, 1065
14 Floyd, S., Heiskanen, T., Taylor, T. W., Mann, G. E. and Ray, W. H. *J. Appl. Polym. Sci.* 1987, **33**, 1021
15 Floyd, S., Choi, K. Y., Taylor, T. W. and Ray, W. H. *J. Appl. Polym. Sci.* 1986, **32**, 2935
16 Laurence, R. L. and Chiovetta, M. G. in 'Proceedings of the Berlin Workshop on Polymer Reaction Engineering' (Eds K. H. Reichert and W. Geisler), Hans Verlag, Munich, 1982, p. 73
17 Yuan, H. G., Taylor, T. W., Choi, K. Y. and Ray, W. H. *J. Appl. Polym. Sci.* 1982, **27**, 1691
18 Sarkar, P. and Gupta, S. K. *Polymer* 1991, **32**, 2842
19 Sarkar, P. and Gupta, S. K. *Polymer* 1992, **33**, 1477
20 Sarkar, P. PhD dissertation, Indian Institute of Technology, Kanpur, India, 1992
21 Treybal, R. E. 'Mass Transfer Operations', 3rd Edn, McGraw-Hill, New York, 1980, pp. 153–157
22 Perry, R. H., Green, D. W. and Maloney, J. O. 'Perry's Chemical Engineers' Handbook', 6th Edn, McGraw-Hill, New York, 1984
23 McCabe, W. L., Smith, J. C. and Harriott, P. 'Unit Operations of Chemical Engineering', 4th Edn, McGraw-Hill, New York, 1985, pp. 142–143
24 Scheibel, E. G. *Ind. Eng. Chem.* 1954, **46**, 2007
25 Wilke, C. R. and Chang, P. *AIChE J.* 1955, **1**, 264
26 Soave, G. *Chem. Eng. Sci.* 1972, **27**, 1197
27 Daubert, T. E. 'Chemical Engineering Thermodynamics', McGraw-Hill, New York, 1987, p. 406
28 Sarkar, P. and Gupta, S. K. *Polym. Eng. Sci.* 1992, **32**, 732
29 Albright, L. F. 'Processes for Major Addition-Type Plastics and Their Monomers', McGraw-Hill, New York, 1974

NOMENCLATURE

a_{gl} Gas–liquid interfacial area per unit volume of liquid and gas bubbles ($m^2\ m^{-3}$)
a_{ls} Liquid–solid interfacial area per unit volume of solid (macroparticles) and liquid ($m^2\ m^{-3}$)
C^* Catalyst active site concentration (mol site $(m^3$ catalyst$)^{-1}$)
C_D Drag coefficient
d_g Diameter of gas bubble (m)
d_i Impeller diameter (m)
d_s Diameter of the solid macroparticle (m)
d_t Diameter of the reactor (m)
$D_{ef,i}$ Effective macroparticle diffusivity at the ith grid point ($m^2\ s^{-1}$)
D_l Diffusivity of solute propylene in liquid n-heptane ($m^2\ s^{-1}$)
D_n Concentration of dead polymer having n monomer units (mol $(m^3$ catalyst$)^{-1}$)
D_s Effective monomer diffusivity in pure (solid) polymer ($m^2\ s^{-1}$)
DP Degree of polymerization
$\overline{DP}$ Mean degree of polymerization in the macroparticle
g Acceleration due to gravity ($m\ s^{-2}$)
h Height of liquid in the reactor (m)
$[H_2]$ Hydrogen concentration (uniform inside macroparticles) (mol m^{-3})
k_{gl} Liquid-side mass transfer coefficient at the gas–liquid interface ($m\ s^{-1}$)
k_{ls} Liquid-side mass transfer coefficient at the liquid–solid interface ($m\ s^{-1}$)
k_p Rate constant for propagation (m^3 (mol site)$^{-1}$ s^{-1})
k_{tr} Rate constant for termination ($m^{3/2}\ mol^{-1/2}\ s^{-1}$)
M_i Monomer concentration at the ith grid point (mol m^{-3})
M_l Concentration of propylene in the (bulk) liquid (mol m^{-3})
$M_{l,i}^*$ Equilibrium concentration of propylene at the gas–liquid interface at a given pressure and temperature (mol m^{-3})
M_n Number-average molecular weight
$\overline{M}_n$ Mean number-average molecular weight of polymer in the macroparticle
$M_{n,k}$ Number-average molecular weight in the kth shell
M_{N+2} Concentration of propylene at the outer surface of the solid at any time (mol m^{-3})
M_w Weight-average molecular weight
$\overline{M}_w$ Mean weight-average molecular weight of polymer in the macroparticle
$M_{w,k}$ Weight-average molecular weight in the kth shell
MW Molecular weight of propylene (kg mol^{-1})
N Initial number of shells in the macroparticle
N_i Number of catalyst fragments in the ith shell
N_s Impeller speed (rev s^{-1})
N_0 Total number of catalyst macroparticles in the reactor
P_{max} Maximum allowable pressure at the top of the reactor (Pa)
P_n Concentration of sites with a growing chain of n monomeric units (mol $(m^3$ catalyst$)^{-1}$)
P_t Pressure at the top of the reactor (Pa)
P_0 Concentration of empty sites (mol $(m^3$ catalyst$)^{-1}$)
q_{exit} Rate of propylene exiting from the reactor (mol s^{-1})

$q_{m,in}$ Rate of monomer bubbled into the reactor (mol s^{-1})
$q_{m,out}$ Rate of monomer going out from the slurry to the vapour space at the top of the reactor (mol s^{-1})
Q Polydispersity index
$\bar{Q}$ Mean polydispersity index of polymer in the macroparticle
r Radial position (m)
R Radius of the macroparticle at any time (m)
$\mathbb{R}$ Universal gas constant (J mol^{-1} K^{-1})
$R_{c,i}$ Radius of catalyst fragment in the ith shell (m)
$\mathscr{R}_i$ Rate of reaction per unit volume at the ith grid point (mol m^{-3} s^{-1})
R_{N+2} Macroparticle radius (m)
R_0 Initial catalyst macroparticle radius (m)
Ra Raleigh number (dimensionless)
Re_g Reynolds number for a gas bubble (dimensionless)
Re_s Reynolds number of the solid macroparticle (dimensionless)
Re_t Reynolds number based on impeller diameter $d_i^2 N_s \rho_l / \mu_l$ (dimensionless)
Sc Schmidt number
Sh_{gl} Sherwood number for the gas–liquid interface (liquid side) (dimensionless)
Sh_{ls} Sherwood number for the liquid–solid interface (liquid side) (dimensionless)
t Time (s)
t_{end} Reaction time (s)
T Temperature of the reactor (K)
u_{term} Terminal settling velocity of the macroparticle (m s^{-1})
v_g Superficial inlet gas velocity (m s^{-1})
v_{term} Terminal velocity of gas bubble (m s^{-1})
V^* Volume of gas at the top of the reactor (m^3)
$V_{c,i}$ Critical molar volume of the ith component (m^3 mol^{-1})
V_g Total volume of the gas bubble phase (m^3)
V_i'' Liquid molar volume of the ith component at its normal boiling point (m^3 mol^{-1})
V_l Total volume of the liquid in the reactor (m^3)
V_s Total volume of the solid in the reactor (m^3)
W Power delivered by the impeller in the absence of sparging (W)
W_g Power delivered by the impeller in the presence of sparging (W)
W_k Mass fraction of polymer in the kth shell
α Probability of propagation
ε^* Void fraction of close-packed spheres ($=0.476$)
λ_k kth moment of live polymer (P_n) MWD
Λ_k kth moment of dead polymer (D_n) MWD
μ_g Viscosity of gaseous propylene (Pa s)
μ_l Viscosity of the pure liquid medium (nC_7) (Pa s)
ρ_c Density of catalyst (kg m^{-3})
ρ_l Density of liquid (nC_7) (kg m^{-3})
ρ_p Density of polymer (kg m^{-3})
σ Surface tension of the liquid (nC_7) (N m^{-1})
ϕ_g Volume fraction of gas bubbles in the liquid